
HOW TO SELECT SLICES FOR ANNOTATION TO TRAIN BEST-PERFORMING DEEP LEARNING SEGMENTATION MODELS FOR CROSS-SECTIONAL MEDICAL IMAGES?

© **Yixin Zhang**

Department of Electrical and Computer Engineering
Duke University
Durham, NC 27708, USA
yixin.zhang7@duke.edu

Kevin Kramer

Minnesota Health Solutions
Minneapolis, MN 55414, USA
kevin@minnhealth.com

Maciej A. Mazurowski*

Department of Radiology
Duke University
Durham, NC 27708, USA
maciej.mazurowski@duke.edu

ABSTRACT

Automated segmentation of medical images highly depends on the availability of accurate manual image annotations. Such annotations are very time-consuming and costly to generate, and often require specialized expertise, particularly for cross-sectional images which contain many slices for each patient. It is crucial to ensure the best use of annotation resources. In this paper, we systematically answer the question of how to select slices of cross-sectional medical images in order to maximize performance of the resulting deep learning segmentation models. We conducted experiments on 4 medical imaging segmentation tasks with varying annotation budgets, numbers of annotated cases, numbers of annotated slices per volume, slice selection techniques, and mask interpolations. We found that: 1) It is almost always preferable to annotate fewer slices per volume and more volumes given an annotation budget. 2) Selecting slices for annotation by unsupervised active learning (UAL) is not superior to selecting slices randomly or at fixed intervals, provided that each volume is allocated the same number of annotated slices. 3) Interpolating masks between annotated slices rarely enhances model performance, with exceptions of some specific configuration for 3D models.

Keywords Deep Learning · Medical Imaging · Annotation · Semantic Segmentation

1 Introduction

Convolutional Neural Networks (CNNs) and Visual Transformers (ViTs) are leading architectures in deep learning for image processing due to their high performance. However, their training requires large, annotated datasets, which are frequently unavailable in medical imaging. Although fine-tuning models that have been pre-trained on extensive natural image datasets (such as COCO, ImageNet, or ADE20K) appears promising, Alzubadi et al. demonstrated that these models might only capture limited features from CT/MRI images due to differences in feature spaces between natural and medical images. [1] As a result, researchers often need to create new annotations for their specific medical imaging tasks.

*The author holds secondary appointment in Department of Electrical and Computer Engineering, Department of Computer Science, Department of Biostatistics & Bioinformatics at Duke University.

Budget constraints typically restrict the number of slices that can be annotated per 3D volume. As a result, researchers use "sparse annotation", where only a subset of slices is annotated to reduce annotators' workload. Çiçek et al. found that 3D-UNet trained on sparse annotations can perform comparably to those trained on dense annotations for kidney segmentation. [2] However, the optimal number of volumes and slices per volume to be annotated remains unclear; the effectiveness of sparse annotation across diverse types of objects is also untested. Our study iterates through various annotation configurations and target object types to answer these questions.

Another practice relevant to model training with sparse annotations is to generate dense annotations from sparse ones, which we refer to as mask interpolation. Yeung et al. introduced Sli2Vol, a self-supervised framework that reconstructs annotations for unlabeled slices based on a reference slice, converting sparsely annotated volumes into densely annotated ones with a combination of human-annotated and algorithm-generated masks. [3] Wu et al. proposed Single Slice Annotation (SSA) with similar purpose but incorporated more sophisticated pre-processing and regularization during model training for better robustness. [4] While these methods do not offer complete code that can be used in a plug-and-play manner, our implementation based on these approaches achieved comparable performance in mask interpolation. We evaluate whether this interpolation adds value under various conditions.

Choosing which slices to annotate within each volume is also plausibly an important aspect that will affect model performance. We empirically compared the efficacy of three slice sampling methods. Two of the methods, fixed-interval and uniform-random sampling, are simple yet effective for unbiased slice sampling with a wide coverage of locations within each volume.

A third approach to slice selection leverages the concept of Active Learning (AL) [5][6][7], which seeks to reduce labeling costs by focusing on the most informative samples. However, traditional AL methods often require extensive human-computer interaction, and/or the availability of some advanced data engines with UI, making them difficult to deploy in many settings. To address this drawback under a research setting (e.g. universities, hospitals), we implemented a variant of AL based on Unsupervised Active Learning (UAL). This class of methods claim to preserve the key advantage of selecting the "most informative or representative subset of samples" within a fixed annotation budget, while eliminating the need for human interaction with the model during the slice selection process. [8][9][10]

Based on the aspects we mentioned, our experiments adhere to the following assumptions:

1. Annotations are performed on slices aligned along the axial axis (Superior-Inferior direction).
2. Supervised training begins only after the full set of annotations is complete.
3. All voxels in the dataset have consistent physical spacing.
4. An equal number of slices are chosen from each volume.
5. The cost of annotating each slice is consistent.

These experiments aim to provide researchers with detailed insights, enabling more precise and well-informed decisions in configuring sparsely annotated datasets for model training. A related but different topic to our work is weakly supervised learning (WSSS) [11][12][13]. Under a broad definition, model training with sparse annotations can be viewed as a subset of weakly supervised learning at the volume or scan level. However, our study assumes that each selected slice is perfectly annotated, with the primary focus on analyzing the trade-offs between the density of annotations per volume and the total number of distinct volumes included in the training set. Additionally, we do not include self-supervised learning in our scope, as models in practice consistently use pre-trained weights from existing models trained on similar anatomical structures, making this consideration unnecessary for our analysis.

2 Methods

2.1 The three primary dimensions of interest

Our research aims to offer guidance on how to annotate 3D volumes effectively when faced with annotation budget constraints. We address this issue through three primary dimensions.

2.1.1 Fewer Annotated Slices Per Volume for More Volumes or More Annotated Slices Per Volume for Less Volumes?

We explored whether it is more advantageous to annotate a few volumes with more annotated slices per volume or to spread annotations across a larger number of volumes with fewer annotated slices per volume. To simplify the description, we define the parameters involved in this experiment as annotation density (ρ) and volume count (s), respectively. Annotation density (ρ) represents the percentage of annotated slices per volume. It takes values from the

set $\{5\%, 10\%, 20\%, 40\%, 80\%\}$. Volume count (s) represents the fraction of volumes with annotations from all volumes reserved in the original training set. It takes value from the set $\{1/8, 1/4, 1/2, 1/1\}$. For a dataset configuration with ($\rho=10\%$, $s=0.25$), one-fourth of all available training volumes are selected for this dataset, and 10% slices per selected volume are annotated. Multiplying annotation density and volume count will then give the total annotation budget as the fraction of the budget for all volumes and all slices.

For all segmentation tasks, we created the sparsely annotated datasets by iterating through all combinations of parameter pairs (ρ, s). We trained models on these datasets three times for each unique set of hyper-parameters, and then compared their average performance (IoU). In this experiment, for each chosen budget level, we report the average performance across the different (ρ, s) combinations using the three slice sampling methods.

2.1.2 Impact of Mask Interpolation (M.I.)

We also examined whether interpolating masks between annotated slices before training improves model performance in both 2D and 3D segmentation settings. We first verified that our implementation of M.I. achieved comparable performance to Sli2Vol [3] and SSA [4] on organ-like objects. Following the procedure outlined in Algorithm 1, we generated pseudo-masks for the unannotated slices in a sparsely annotated dataset.

Algorithm 1 Slices with Human Annotations

```

1:  $pos\_queue \leftarrow \{\text{human annotated masks}\}$ 
2: while  $pos\_queue$  is not empty do
3:    $mask_i \leftarrow pos\_queue.dequeue()$ 
4:    $mask_{i-1}, mask_{i+1} \leftarrow mask\_prop(slices_i, mask_i)$ 
5:   if  $slice_{i-1}$  is new and  $slice_{i-1}$  contains object then
6:      $pos\_queue.addback(mask_{i-1})$ 
7:   end if
8:   if  $slice_{i+1}$  is new and  $slice_{i+1}$  contains object then
9:      $pos\_queue.addback(mask_{i+1})$ 
10:  end if
11: end while
12: Assign 0 to the rest of the unannotated slices.
```

With the setup using all volumes ($s=1$), we vary the annotation density ρ to evaluate whether, and under what conditions, models trained with M.I. yield better performance compared to those that ignore the gradients of unannotated slices or voxels. We report on the quality of the interpolated mask based on its IoU with the corresponding human annotation, and compare model performance on the same sparsely annotated volumes, both with and without the M.I. technique.

2.1.3 Impact of Slice Sampling Methods within Volumes

Assuming a fixed configuration of annotation density (ρ), volume count (s), we examined different ways of selecting slices for annotation impact model performance. The methods of selection considered are:

1. Selection at fixed interval (i.e., annotating every n -th slice)
2. Selection at uniform random (i.e., randomly picking slices with uniform distribution)
3. Selection by UAL (i.e., using a “smart” way to select samples)

For each (ρ, s) configuration, we train three models on datasets with annotated slices selected by the aforementioned sampling methods. We measure each model’s performance relative to the triplet’s average and display the results in a bar plot. If a slice selection method is superior, its bar should be noticeably higher than the others for the same dataset.

2.2 Datasets

Our experiments involved three datasets across four tasks. Table 1 summarizes the dataset specifications after preprocessing, ensuring all annotated volumes have uniform dimensions and consistent voxel spacing.

2.3 Model Training

The model architecture and hyper-parameters paired with each dataset are listed in Table 2. We selected various variants of representative segmentation models commonly used in the computer vision community and paired them with each

Dataset	Target	Voxel Spacing (mm)	Dimensions	#Train	#Val	#Test
LiTS17[14]	Liver tumor	(1, 1, 1)	384×384×384	96	10	25
DBC-Breast[15]	Breast	(0.7, 0.7, 1)	496×496×176	72	8	20
DBC-FGT[15]	Fibroglandular Tissue	(0.7, 0.7, 1)	496×496×176	72	8	20
ATLAS[16]	Lesions	(1, 1, 1)	224×256×189	500	55	100

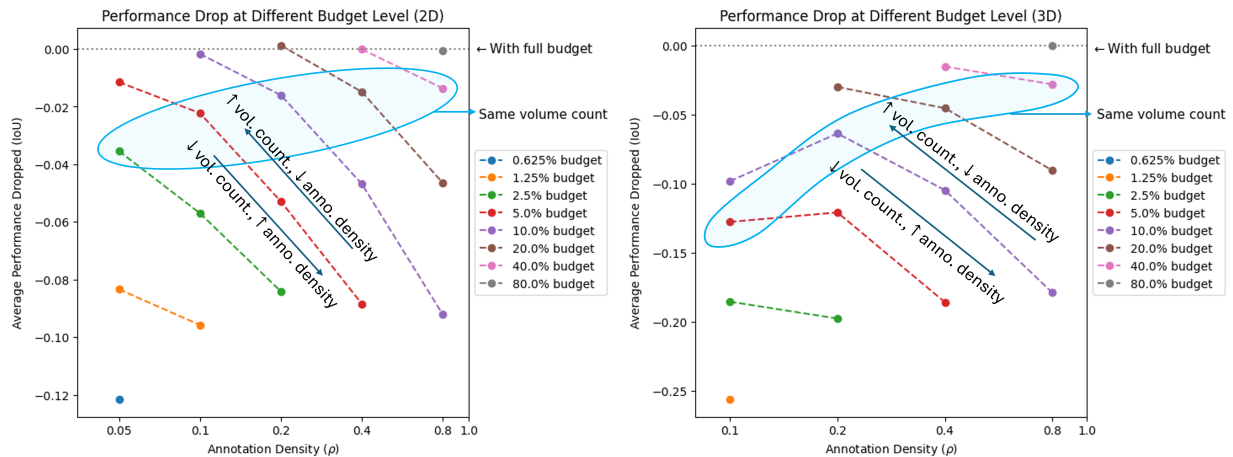
Table 1: Specifications of the 3D volumes after preprocessing in each dataset

dataset based on its level of difficulty. In other words, more challenging datasets were matched with models having larger parameter sizes and greater prediction capabilities. This approach allows us to cover a wide range of training settings and datasets without having to repeat experiments across all possible (dataset-model) combinations. The hyper-parameters for model training were tuned using the original densely annotated dataset to ensure that model performance falls within the operational range reported in existing literature for similar tasks. In our 2D segmentation experiments, we ensure that samples in each batch are drawn uniformly at random from the annotated slices across all datasets to maintain consistency. For 3D segmentation, we implement different sampling strategies based on the dataset. In LiTS17, we sampled patch centers with a 50% probability for liver, 30% for tumor, and 20% for background or unannotated voxels to focus on the areas of interest. For the DBC and FGT datasets, patch centers are sampled randomly without specific probabilistic constraints. In the ATLAS dataset, we sample patch centers with a 30% probability for background, 55% for lesions, and 15% for unannotated voxels to ensure a diverse representation of the different regions. These sampling strategies are designed to optimize the training process by effectively representing the various anatomical features and ensuring balanced learning. The results of these experiments will be detailed in the following section.

3 Results

3.1 Fewer Annotated Slices Per Volume for More Volumes or Converse?

3.1.1 2D Segmentation Setting



(a) Average performance disparity for 2D models

(b) Average performance disparity for 3D models

Figure 1: Average model performance drops when sparsely annotated datasets with different annotation density and volume counts are used for trained 2D (Fig.1a) and 3D (Fig.1b) models. Volume counts are adjusted to match the annotation budget.

Fig. 1 presents the performance of models trained on sparsely annotated datasets relative to those trained on densely annotated counterparts, averaged across all datasets for different(ρ, s) configurations. This figure highlights an important

¹Model weight is initialized from the MiT-B3 pretraining

²The VGG16 encoder in the coarse-segmentation module is initialized from ImageNet-pretrained weights

Settings for 2D Models, all models set batch size to 16						
Dataset	Data Augmentation	Loss Function	Optimizer	LR Scheduler	Iterations	
LiTS17 Inception-UNet [17]	RandomBiasField, ElasticDeformation, RandomFlip	Weighted CE at [0.04, 0.25, 1.4]	AdamW w/ lr=1e-4, weight_decay =1e-5	Polynomial w/ power=0.8	14000	
DBC-FGT SegFormer-B3 ¹ [18]	Duplicate grayscale to RGB, RandomFlip	Cross Entropy	AdamW w/ lr=1e-4, weight_decay =1e-2	Polynomial w/ power=0.8	12000	
ATLAS CAM- Wnet ² [19]	RandomFlip	Soft Dice and Cross Entropy	AdamW w/ lr=5e-5, weight_decay =1e-5	Exponential w/ $\gamma = 0.7$ per 2000 iterations	15000	
Settings for 3D Models (all models were trained from scratch)						
Dataset	Data Aug.	Loss Function	Optimizer	LR Scheduler	Iterations	Patch Size
LiTS17 3D-UNet [2]	RandomBiasField, RandomAffine, RandomFlip	Weighted CE at [0.04, 0.2, 1.0]	SGD w/ lr=1e-2, weight_decay =1e-4, momentum =0.9	None	18000 (batch=24)	128×128×128 resized to 64×64×64
DBC-FGT SegResNet [20]	RandomAffine, RandomFlip	Cross Entropy	Adam w/ lr=3e-4, weight_decay =1e-5	Cosine Annealing	12000 (batch=24)	128×128×64
ATLAS UNETR [21]	RandomAffine, RandomFlip	Dice Focal Loss	AdamW w/ lr=1.5e-4, weight_decay =1e-6	Exponential w/ $\gamma = 0.7$ per 3000 iterations	15000 (batch=54)	96×96×64

Table 2: Model architecture, data augmentation and training hyper-parameters used for each dataset. All augmentations were implemented in TorchIO [22].

observation: under 2D segmentation setting, regardless of the total annotation budget, it is consistently more advantageous, in terms of model performance, to annotate more volumes with fewer slices per volume, provided that the total number of annotated slices remains constant. This finding also holds across all levels of annotation density. In fact, the impact of the density of the annotated volume on performance was generally quite low. This means that annotations of many slices could be skipped with very low loss in performance (until the density is less than 0.2). The driving factor for model performance was clearly the number of volumes which contained annotations.

For LiTS17 (Liver Tumor Segmentation, Fig. 2a, 2e), higher annotation density (ρ) consistently resulted in lower performance when compared to increasing volume counts, regardless of the budget. Doubling ρ did not improve performance as effectively as doubling the volume count (s). The same performance trend observed in LiTS17-tumor was seen in both tasks of the DBC-FGT datasets (Fig. 2b, 2c, 2f, 2g). For these tasks, improving performance was more effectively achieved by increasing the volume count rather than the annotation density.

In the ATLAS dataset (Brain MRI, Fig. 2d, 2h), we also observed a trend not captured in the previous few datasets at four budget levels (1181, 2362, 4725, and 37800 slices): some lower volume count configurations achieved comparable or even superior performance. There are two cases for such exception, one occurs when both the total budget and annotation density are small (i.e., budget ≤ 4725 slices, $\rho \leq 0.1$). The other occurs when both the total budget and annotation density are large (i.e., budget ≥ 37800 slices, $\rho \geq 0.4$).

Based on these results, if a dataset is prepared for training 2D models, spreading annotation budgets across more volumes at diverse locations is always more cost-effective. A small annotation density (e.g., 5% \sim 20% slices labeled) is often sufficient for training models with similar performance to the counterparts trained with the full dataset.

³The 3D setting excluded the data points for $\rho=0.05$ because some model instances failed to converge at this configuration

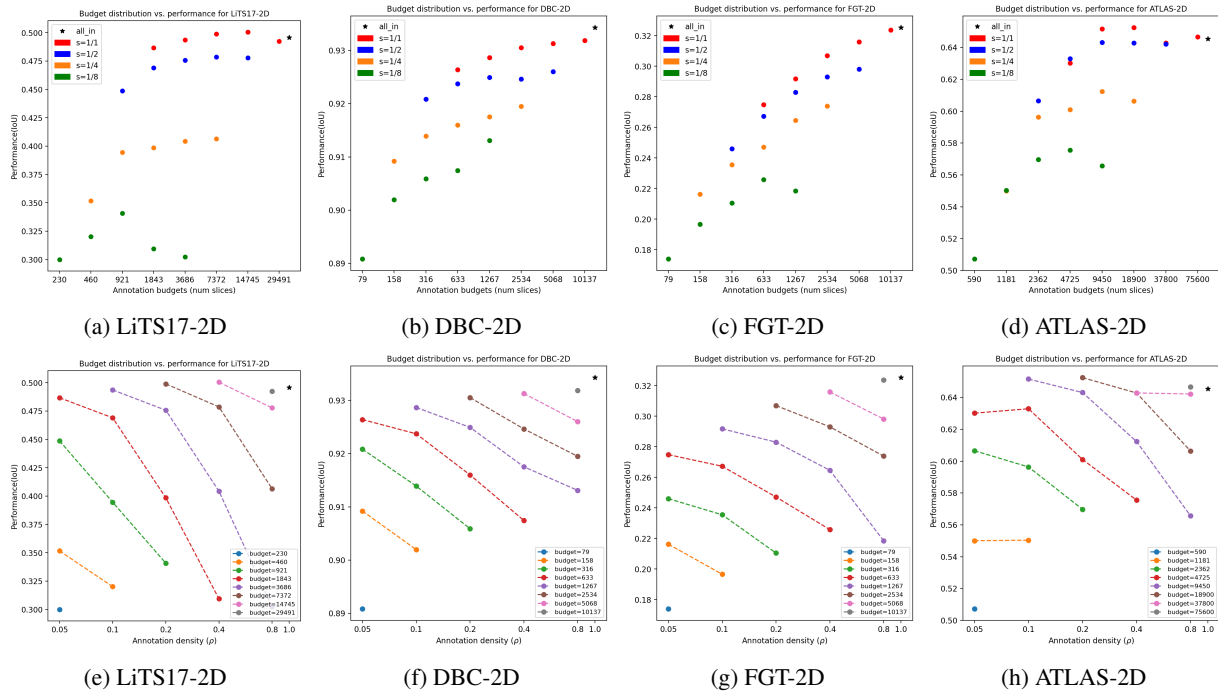


Figure 2: (a)-(d): Performance (y-axis, by IoU) of 2D models when trained on sparsely annotated datasets with different configurations of annotation budget (x-axis) and volume count (by color). (e)-(h): Performance of 2D models trained with different (annotation density, volume count) configurations. Points on the same line (same color) consume the same budgets (i.e., annotated slices).

3.1.2 3D Segmentation Setting

In the 3D segmentation setting, most patterns observed in the 2D models also apply, but with some notable differences. As shown in Fig. 1b, we observed that excessively low annotation density can hinder model performance in certain conditions.

For LiTS17-tumor and DBC-FGT tasks in 3D, the trends mirror those in 2D (Fig. 3a, 3b, 3c, 3e, 3f, 3g): low annotation density does not significantly affect performance due to clear object-background contrast. However, for the ATLAS dataset, the behavior was slightly different. At low annotation density $\rho = 0.05$, the model failed to learn useful features and showed no prediction capability, thus omitted in our report. Instead, increasing annotation density in the range of $0.1 \leq \rho \leq 0.4$ led to noticeable performance improvements, as shown in Fig. 3d, 3h.

3.2 Should Mask Interpolation Be Used?

We examined whether imputing labels for unannotated voxels before training provides an advantage over training directly with sparse annotations. Table 4 presents the IoUs between interpolated dense annotations and their human-annotated counterparts across different annotation densities.

In 2D segmentation, mask interpolation had minimal impact on model performance across all datasets. In 3D segmentation, the effects varied: for DBC breast segmentation, the impact was minimal, while LiTS17 tumor segmentation often experienced a performance drop, particularly at low annotation densities ($\rho = 0.05$). Significant performance drops were noted with FGT (fibro-glandular tissue segmentation). This may be due to loss of tissue details in interpolated masks, such as gaps and spaces in tree-like structures, yet the reason for the lack of performance drop in 2D cases remains unclear. Conversely, ATLAS showed improved performance at low annotation densities ($\rho \leq 0.2$), indicating that mask interpolation can be beneficial for certain types of objects.

⁴The interpolated volumes for ATLAS assumed positive weight stratification to ensure convergence. At an annotation density of 0.8, all positive slices may be pre-annotated.

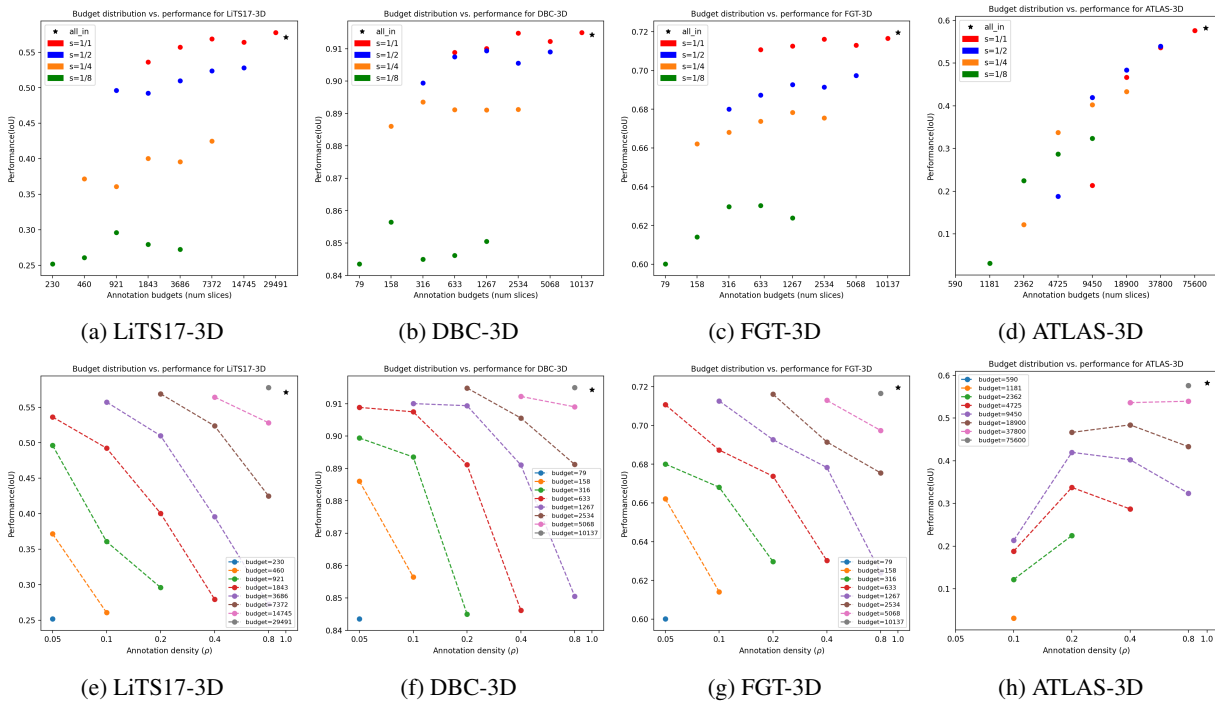


Figure 3: (a)-(d): Performance (y-axis, by IoU) of 3D models when trained on sparsely annotated datasets with different configurations of annotation budget (x-axis) and volume count (by color). (e)-(h): Performance of 3D models trained with different (annotation density, volume count) configurations. Points on the same line (same color) consume the same budgets (i.e., annotated slices).

Annotation Density (ρ)	0.05	0.1	0.2	0.4	0.8
LiTS17	0.9079	0.9431	0.9683	0.9931	0.9926
DBC	0.9673	0.9781	0.9856	0.9912	0.9971
ATLAS	0.5621	0.7326	0.8831	0.9674	N/A ⁴
FGT	0.6366	0.7118	0.7763	0.8447	0.9456

Table 3: Quality of dense annotation interpolated from sparse annotation at different densities (ρ).

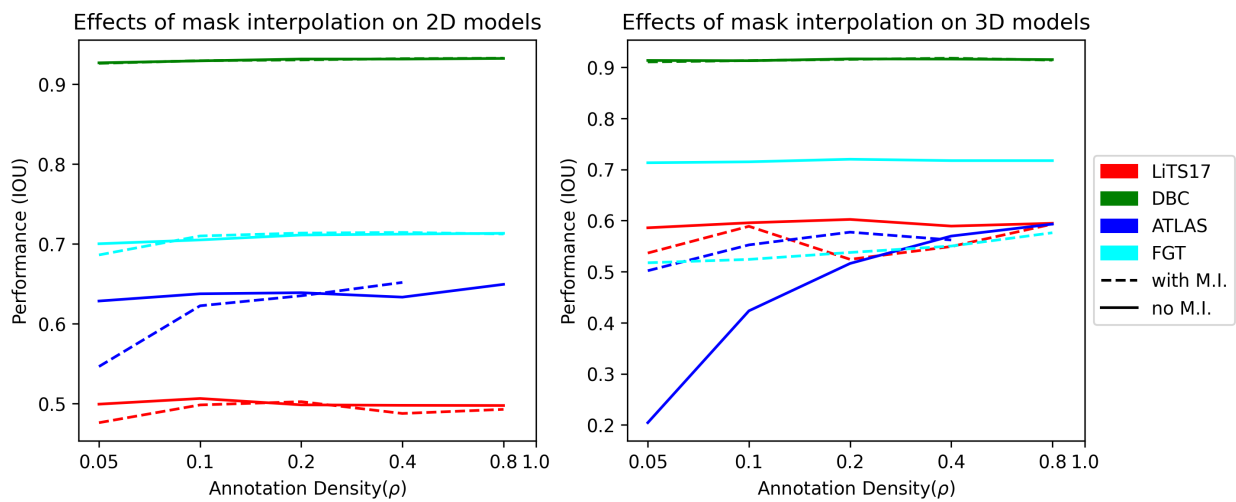


Figure 4: Model performance when trained on the same set of annotated slices with and without the use of mask interpolation. Only for 3D model trained on ATLAS with $\rho \leq 0.4$ (low annotation density) showed improved model performance via Mask Interpolation(M.I.).

3.3 Is the way slices are selected for annotation important?

In the previous section, we compared how the trade-off between annotation density and volume count affects model performance. Now, we examine the impacts of the different slice selection policies.

Fig. 5 shows that the performance differences between the three slice selection policies are minor. Neither method consistently outperforms the others in 2D or 3D settings. In 3D models, while overall trends are similar to those in 2D, there is greater variation in how different selection policies affect performance.

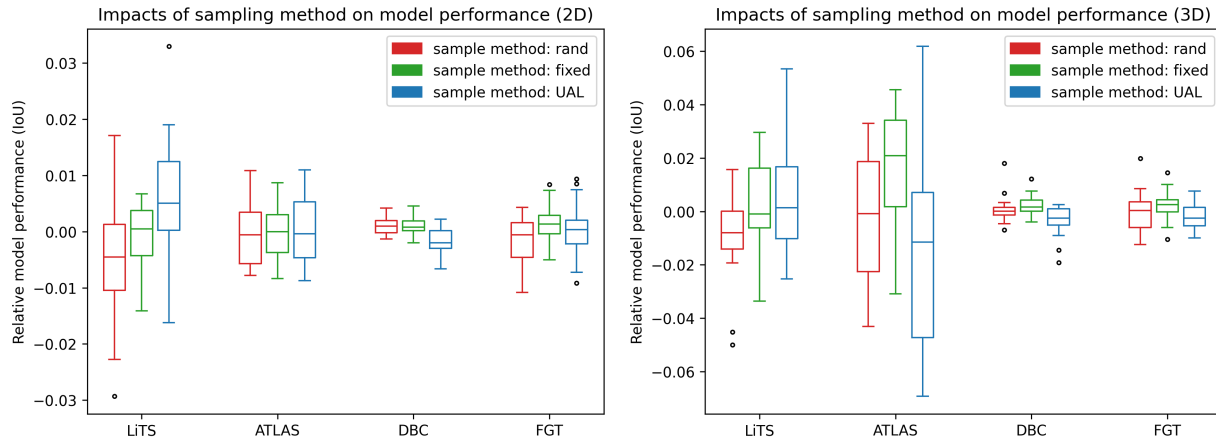


Figure 5: Distribution of relative performance among models trained on the three slices selection policies.

4 Discussion

In our 2D segmentation experiments, we found it advantageous to distribute the annotation budget across a greater number of volumes with fewer annotated slices per volume. This approach helps mitigate redundancy in adjacent slices, as focusing annotation on fewer volumes results in many highly similar slices. Annotating a broader range of volumes introduces the model to a wider variety of variations between volumes, which data augmentation may not replicate. In 3D deep learning methods, the principle that "sparser annotations are better" generally holds true as well. We notice an exception to this rule for the ATLAS dataset when a very low number of slices per volume is annotated. When annotation density falls below 20%, prioritizing a higher volume count over annotation density does not result in improved model performance. Our preliminary data on the topic points to the likely impact of the network architecture (the generally observed trend appears to be maintained when AttentionUNet-3D [23] is used in place of UNETR) and a potential impact of an interaction between this dataset and the architecture. More experiments are needed to further elucidate this exception.

Regarding slice selection policies, we did not find any one method to be significantly superior to the others. All three tested methods produced comparable results. Although previous literature suggests that slice selection by UAL-based algorithms can outperform that at fixed interval or random, this advantage was not consistently observed across all datasets in our study. This discrepancy might be because UAL tends to pick visually distinct slices, which may not always be the most relevant for our segmentation tasks. Additionally, we applied UAL-based selection within each volume to keep the experiment uniform and reduce computational load, rather than across the entire dataset. This method could have limited UAL's effectiveness compared to dataset-level selection, where the latter might better identify and exclude less informative volumes.

Our findings recommend that annotation budgets be distributed across as many volumes as possible for both 2D and 3D segmentation tasks. For 3D cases, it is also important to maintain a minimum number of annotated slices per volume to ensure effective model training and convergence. Since all examined slice selection methods yielded comparable results, slice selection at fixed interval is proved sufficient for simplicity. In our study, we did not include biased selection method such as those including only slices from the beginning of the volume, as we focused on those that would distribute the annotated slices more evenly across the volume. Future studies may explore the impact of violating this assumption, such as if slices were exclusively taken from a single lesion rather than multiple lesions within a volume.

Our study assumed each slice consumes consistent time and resources to annotate. In practice, slices containing target objects are more time-consuming to annotate as compared to the empty counterparts. Also, annotating slices across

multiple volumes can be more challenging than annotating the same number of slices within a single volume due to the additional effort required for frequent switching between images and re-recognizing the context in the images. Future study may explore a more advanced modeling of the resources and time consumed under these settings.

5 Acknowledgments

Research reported in this publication was supported by the National Heart, Lung, and Blood Institute of the National Institutes of Health under Award Number R44HL152825. The content is solely the responsibility of the authors and does not necessarily represent the official views of the National Institutes of Health.

References

- [1] Laith Alzubaidi, Muthana Al-Amidie, Ahmed Al-Asadi, Amjad J. Humaidi, Omran Al-Shamma, Mohammed A. Fadhel, Jinglan Zhang, J. Santamaría, and Ye Duan. Novel transfer learning approach for medical imaging with limited labeled data. *Cancers*, 13(7), 2021. ISSN 2072-6694. doi:10.3390/cancers13071590. URL <https://www.mdpi.com/2072-6694/13/7/1590>.
- [2] Özgün Çiçek, Ahmed Abdulkadir, Soeren S Lienkamp, Thomas Brox, and Olaf Ronneberger. 3d u-net: learning dense volumetric segmentation from sparse annotation. In *Medical Image Computing and Computer-Assisted Intervention—MICCAI 2016: 19th International Conference, Athens, Greece, October 17-21, 2016, Proceedings, Part II 19*, pages 424–432. Springer, 2016.
- [3] Pak-Hei Yeung, Ana I. L. Namburete, and Weidi Xie. Sli2vol: Annotate a 3d volume from a single slice with self-supervised learning. In Marleen de Bruijne, Philippe C. Cattin, Stéphane Cotin, Nicolas Padoy, Stefanie Speidel, Yefeng Zheng, and Caroline Essert, editors, *Medical Image Computing and Computer Assisted Intervention – MICCAI 2021*, pages 69–79, Cham, 2021. Springer International Publishing. ISBN 978-3-030-87196-3.
- [4] Yixuan Wu, Bo Zheng, Jintai Chen, Danny Z. Chen, and Jian Wu. Self-learning and one-shot learning based single-slice annotation for 3d medical image segmentation. In Linwei Wang, Qi Dou, P. Thomas Fletcher, Stefanie Speidel, and Shuo Li, editors, *Medical Image Computing and Computer Assisted Intervention – MICCAI 2022*, pages 244–254, Cham, 2022. Springer Nature Switzerland. ISBN 978-3-031-16452-1.
- [5] Pengzhen Ren, Yun Xiao, Xiaojun Chang, Po-Yao Huang, Zhihui Li, Brij B Gupta, Xiaojiang Chen, and Xin Wang. A survey of deep active learning. *ACM computing surveys (CSUR)*, 54(9):1–40, 2021.
- [6] Yarin Gal, Riashat Islam, and Zoubin Ghahramani. Deep bayesian active learning with image data. In *International conference on machine learning*, pages 1183–1192. PMLR, 2017.
- [7] Zhenxi Zhang, Jie Li, Zhushi Zhong, Zhicheng Jiao, and Xinbo Gao. A sparse annotation strategy based on attention-guided active learning for 3d medical image segmentation. *arXiv preprint arXiv:1906.07367*, 2019.
- [8] Hao Zheng, Yizhe Zhang, Lin Yang, Chaoli Wang, and Danny Z Chen. An annotation sparsification strategy for 3d medical image segmentation via representative selection and self-training. In *Proceedings of the AAAI Conference on Artificial Intelligence*, volume 34, pages 6925–6932, 2020.
- [9] Hao Zheng, Lin Yang, Jianxu Chen, Jun Han, Yizhe Zhang, Peixian Liang, Zhuo Zhao, Chaoli Wang, and Danny Z Chen. Biomedical image segmentation via representative annotation. In *Proceedings of the AAAI Conference on Artificial Intelligence*, volume 33, pages 5901–5908, 2019.
- [10] Ozan Sener and Silvio Savarese. Active learning for convolutional neural networks: A core-set approach. In *International Conference on Learning Representations*, 2018. URL <https://openreview.net/forum?id=H1aTuk-RW>.
- [11] Eugene Vorontsov and Samuel Kadoury. Label noise in segmentation networks: mitigation must deal with bias. In *Deep Generative Models, and Data Augmentation, Labelling, and Imperfections: First Workshop, DGM4MICCAI 2021, and First Workshop, DALI 2021, Held in Conjunction with MICCAI 2021, Strasbourg, France, October 1, 2021, Proceedings 1*, pages 251–258. Springer, 2021.
- [12] Aleksandar Zlateski, Ronnachai Jaroensri, Prafull Sharma, and Frédo Durand. On the importance of label quality for semantic segmentation. In *Proceedings of the IEEE Conference on Computer Vision and Pattern Recognition*, pages 1479–1487, 2018.
- [13] Yixin Zhang, Shen Zhao, Hanxue Gu, and Maciej A Mazurowski. How to efficiently annotate images for best-performing deep learning based segmentation models: An empirical study with weak and noisy annotations and segment anything model. *CoRR*, 2023.

- [14] Patrick Bilic, Patrick Christ, Hongwei Bran Li, Eugene Vorontsov, Avi Ben-Cohen, Georgios Kaissis, Adi Szeskin, Colin Jacobs, Gabriel Efrain Humpire Mamani, Gabriel Chartrand, et al. The liver tumor segmentation benchmark (lits). *Medical Image Analysis*, 84:102680, 2023.
- [15] Ashirbani Saha, Michael R. Harowicz, Lars J. Grimm, Connie E. Kim, Sujata V. Ghate, Ruth Walsh, and Maciej A. Mazurowski. A machine learning approach to radiogenomics of breast cancer: a study of 922 subjects and 529 dce-mri features. *British Journal of Cancer*, 119:508 – 516, 2018. URL <https://api.semanticscholar.org/CorpusID:49902015>.
- [16] Sook-Lei Liew, Bethany P Lo, Miranda R Donnelly, Artemis Zavaliangos-Petropulu, Jessica N Jeong, Giuseppe Barisano, Alexandre Hutton, Julia P Simon, Julia M Juliano, Anisha Suri, et al. A large, curated, open-source stroke neuroimaging dataset to improve lesion segmentation algorithms. *Scientific data*, 9(1):320, 2022.
- [17] Narinder Singh Punn and Sonali Agarwal. Inception u-net architecture for semantic segmentation to identify nuclei in microscopy cell images. *ACM Transactions on Multimedia Computing, Communications, and Applications (TOMM)*, 16(1):1–15, 2020.
- [18] Enze Xie, Wenhai Wang, Zhiding Yu, Anima Anandkumar, Jose M Alvarez, and Ping Luo. Segformer: Simple and efficient design for semantic segmentation with transformers. *Advances in neural information processing systems*, 34:12077–12090, 2021.
- [19] Zhenhong Liu, Hongfang Yuan, and Huaqing Wang. Cam-wnet: An effective solution for accurate pulmonary embolism segmentation. *Medical Physics*, 49(8):5294–5303, 2022. doi:<https://doi.org/10.1002/mp.15719>. URL <https://aapm.onlinelibrary.wiley.com/doi/abs/10.1002/mp.15719>.
- [20] Andriy Myronenko. 3d mri brain tumor segmentation using autoencoder regularization. In *Brainlesion: Glioma, Multiple Sclerosis, Stroke and Traumatic Brain Injuries: 4th International Workshop, BrainLes 2018, Held in Conjunction with MICCAI 2018, Granada, Spain, September 16, 2018, Revised Selected Papers, Part II 4*, pages 311–320. Springer, 2019.
- [21] Ali Hatamizadeh, Yucheng Tang, Vishwesh Nath, Dong Yang, Andriy Myronenko, Bennett Landman, Holger R Roth, and Daguang Xu. Unetr: Transformers for 3d medical image segmentation. In *Proceedings of the IEEE/CVF winter conference on applications of computer vision*, pages 574–584, 2022.
- [22] Fernando Pérez-García, Rachel Sparks, and Sébastien Ourselin. TorchIO: a Python library for efficient loading, pre-processing, augmentation and patch-based sampling of medical images in deep learning. *Computer Methods and Programs in Biomedicine*, page 106236, 2021. ISSN 0169-2607. doi:<https://doi.org/10.1016/j.cmpb.2021.106236>. URL <https://www.sciencedirect.com/science/article/pii/S0169260721003102>.
- [23] Ozan Oktay, Jo Schlemper, Loic Le Folgoc, Matthew Lee, Mattias Heinrich, Kazunari Misawa, Kensaku Mori, Steven McDonagh, Nils Y Hammerla, Bernhard Kainz, Ben Glocker, and Daniel Rueckert. Attention u-net: Learning where to look for the pancreas. In *Medical Imaging with Deep Learning*, 2018. URL <https://openreview.net/forum?id=Skft7cijM>.